CHEMISTRY
AN ASIAN JOURNAL
ACES
FULL PAPER

DOI: 10.1002/asia.201300043

Synthesis, Crystal Structures, and Optical/Electronic Properties of Sphere–Rod Shape Amphiphiles Based on a [60]Fullerene–Oligofluorene Conjugate

Fu-Ai Teng,[a] Yan Cao,[b] Yuan-Jiang Qi,[a] Mingjun Huang,[b] Zhe-Wen Han,[a] Stephen Z. D. Cheng,*[b] Wen-Bin Zhang,*[b] and Hui Li*[a]

Abstract: A series of sphere–rod shape amphiphiles, in which a [60]fullerene (C_{60}) sphere was connected to the center of an oligofluorene (OF) rod through a rigid linkage (OF-C_{60}), were designed and synthesized. Alkyl chains of various lengths were attached onto the OFs on both sides of the C_{60} spheres. These compounds, denoted as alkyl-OF-C_{60}, were fully characterized by ^{1}H NMR, ^{13}C NMR, and FTIR spectroscopy and by MALDI-TOF mass spectrometry. The morphologies and structures of their crystals were elucidated by wide-angle X-ray diffraction (WAXD) and by electron diffraction in transmission electron microscopy (TEM). Butyl-OF-C_{60} forms a monoclinic unit cell ($a=1.86$, $b=3.96$, $c=2.24$ nm; $\alpha=\gamma=90°$, $\beta=68°$; space group *P2*), octyl-OF-C_{60} also forms a monoclinic unit cell ($a=2.21$, $b=4.06$, $c=1.81$ nm; $\alpha=\gamma=90°$, $\beta=75.5°$; space group *C2m*), and dodecanyl-OF-C_{60} forms a triclinic structure ($a=1.82$, $b=4.35$, $c=2.26$ nm; $\alpha=93.1°$, $\beta=94.5°$, $\gamma=92.7°$; space group *P1*). The inequivalent spheres and rods were found to pack into an alternating layered structure of C_{60} and OF in the crystals, thus resembling a "double-cable" structure. UV/Vis absorption spectroscopy revealed an electron perturbation between the two individual chromophores (C_{60} and OF) in their ground states. Fluorescence spectroscopy exhibited complete fluorescence quenching of their solutions in toluene, thus suggesting an effective energy transfer from OF to C_{60}. Cyclic voltammetry indicated that the energy-level profiles of C_{60} and OF remained essentially unchanged. This work has broad implications in terms of understanding the self-assembly and molecular packing of conjugated materials in crystals and has potential applications in organic field-effect transistors and bulk heterojunction solar cells.

Keywords: amphiphiles · crystal structures · fullerenes · oligomers · X-ray diffraction

Introduction

Over the past decade, growing recognition of the importance of anisotropy in shape and molecular interactions has led to the development of an exciting field of "shape amphiphiles" for the construction of new functional hierarchical structures.[1] Shape amphiphiles typically refer to hybrids of molecular segments with distinct shapes and competing interactions, and they have been predicted by computer simulations to exhibit rich phase behaviors and various unusual structures, owing to packing constraints and amphiphilic interactions.[2] Typical shape amphiphiles include polymer-tethered nanoparticles, disc–rod mesogenic hybrids, and sphere–cube and disc–cube conjugates,[1a,b,3] in which [60]fullerene (C_{60}) is a common spherical molecular nanoparticle (MNP) building block.[3c,4] Fullerene is an intriguing class of carbon-based MNP with wide-ranging applications, owing to its outstanding electronic properties.[4,5] To better utilize the electronic properties of C_{60}, it is critical to achieve ordered structures of C_{60} in multi-dimensions across different length scales.[6] The self-assembly of fullerene-based shape amphiphiles provides a valuable approach to achieving this goal.[4,7a,b] To tune the formation of these hierarchical structures, precise control over important molecular parameters, such as surface chemistry, chain composition, and polymer architecture, is a prerequisite.[1b,3a,b] In recent years, we have reported the synthesis of a variety of shape amphiphiles based on C_{60}, such as C_{60}-end-capped polymers[8] and sphere–cubic molecules of polyhedral oligomeric silsesquioxane-C_{60}.[4] It is interesting to investigate the self-assembly of sphere–rod shape amphiphiles based on conjugates of

[a] F.-A. Teng,[+] Y.-J. Qi, Prof. Z.-W. Han, Prof. H. Li
School of Materials Science and Engineering
East China University of Science and Technology
Shanghai, 200237,(P. R. China)
Fax: (+86) 21-6425-3163
E-mail: lihui@ecust.edu.cn

[b] Dr. Y. Cao,[+] M. Huang, Prof. S. Z. D. Cheng, Dr. W.-B. Zhang
Department of Polymer Science
College of Polymer Science and Polymer Engineering
The University of Akron, Akron, OH 44325-3909 (USA)
Fax: (+1)-330-972-8626
E-mail: scheng@uakron.edu
wz8@uakron.edu

[+] These authors contributed equally to this work.

Supporting information for this article is available on the WWW under http://dx.doi.org/10.1002/asia.201300043.

C_{60} and conjugated oligomers/polymers, in particular shape-persistent molecules that are connected through a rigid linkage.[9] The synthesis of such shape amphiphiles has been extensively reported, mainly as "double-cable" polymers that are expected to self-assemble into a bicontinuous network with nanophase-segregated electron- and hole-transporting channels for applications in bulk heterojunction organic solar cells.[9,10] However, to the best of our knowledge, there are relatively few reports on the formation of self-assembled ordered structures from these conjugates.[11] In fact, the large inequivalence in terms of molecular conformation and chemical composition between C_{60} and conjugated molecules makes the hybrid difficult to pack into an ordered structure.[10a,12] It is also the lack of control in creating ordered secondary structures that probably accounts for the poor performance of traditional "double-cable" polymers in organic photovoltaic devices.[7,13] To shed light on this system, the "oligomer approach" was adopted to study the self-assembly and properties of well-defined, monodispersed oligomeric conjugated molecule–C_{60} hybrids.[14] Facilitated by breakthroughs in metal-catalyzed cross-coupling synthetic methods, uniform and monodispersed π-conjugated oligomers can now be synthesized with ease.[15] With molecular contour lengths that are typically equal to or less than the exciton-diffusion lengths of organic semiconductors, these conjugated hybrids are unique model systems that can reveal the basic physical principles that underlie their structure–property relationships.[16]

Herein, we report the design, synthesis, crystal structures, and optical/electronic properties of a series of sphere–rod shape amphiphiles based on C_{60}–oligofluorene (OF) conjugates with alkyl side chains of different lengths at the 9 position of the fluorene units and a rigid linkage between C_{60} and OF (Scheme 1). The crystal structures exhibit an alternating layered packing structure of C_{60} and OF with unit-cell symmetry and parameters that are influenced by the length of the alkyl side chains. These results are expected to have broad implications in the understanding of the principles that govern the self-assembly and physical structures of conjugated molecule–C_{60} hybrids.

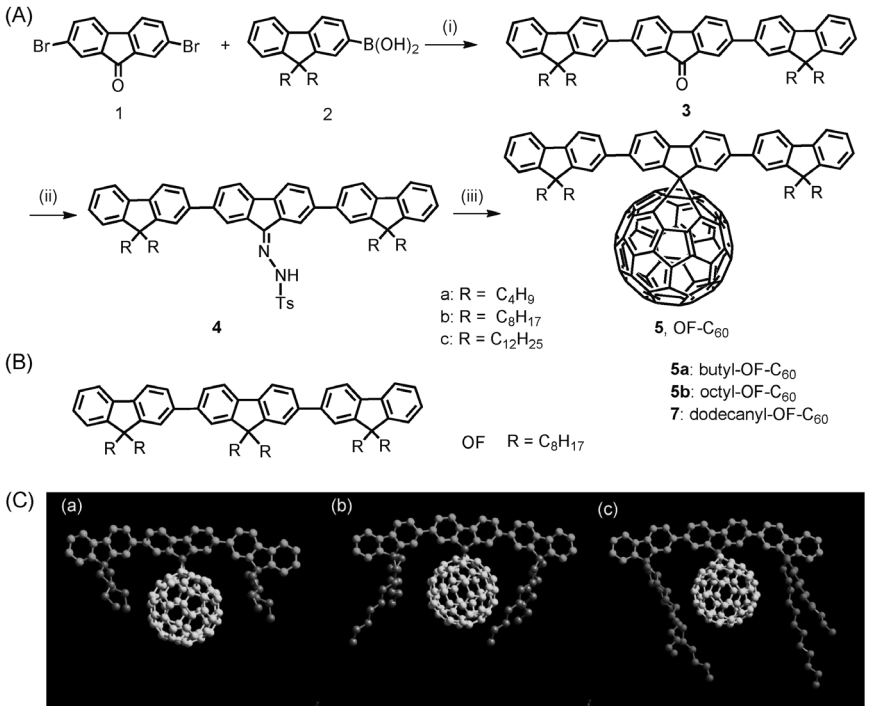

Scheme 1. A) Synthesis of OF-C_{60} shape amphiphiles. Reagents and conditions: (i) $[Pd(PPh_3)_4]$, aq. Na_2CO_3 (2 M), 90 °C, 2 d, 92%; (ii) *p*-toluenesulfonyl hydrazide, THF, HCl (cat.), 80 °C, 7 h, 89%; (iii) sodium methoxide, pyridine, C_{60}, *o*-dichlorobenzene, 80 °C 24h, then reflux, 24 h, 35%. B) Structure of the oligofluorene (OF) trimer as a control sample for the study of the optical and electronic properties of OF-C_{60}. C) Molecular models of butyl-OF-C_{60} (a), octyl-OF-C_{60} (b), and dodecanyl-OF-C_{60} (c).

Results and Discussion

Molecular Design and Synthesis of OF-C_{60} Dyads

Hybrids of C_{60} and various conjugated materials, such as oligo-*p*-phenylenevinylenes, oligothienylenevinylenes, oligo-*p*-phenylene-ethynylenes, and oligothiophenes, have been extensively reported over the past two decades.[12,14a] Among the commonly used conjugated compounds, oligofluorene (OF) is a hole-transporting material with high charge mobility that has been widely used as a model rod-like π-conjugated supramolecular building block.[17] Caporossi et al. reported the synthesis of two fluorene–C_{60} dyads in which the C_{60} balls were linked at the 2 and 9 positions of the fluorene unit, respectively.[18] Martin and co-workers reported the synthesis of two series of OF-C_{60} dyads, with one or two C_{60} spheres capping the end(s) of the OF.[19] However, to the best of our knowledge, there are no systematic studies on the self-assembled ordered structures of such hybrids, owing to, in part, the high inequivalence between the two components in terms of their shape and interactions, as well as strong aggregation between the C_{60} spheres, which complicates the formation of ordered structures. In other words, the aggregation of C_{60} spheres and their rigid 3D shape make the formation of an ordered structure difficult. In general, there are two strategies to overcome this difficulty: 1) The introduction of molecular moieties with a stronger capability for structure formation so as to override the ag-

gregation of C_{60} and to serve as a template to induce the ordered packing of C_{60} spheres; and 2) the linking of C_{60} spheres to the other structure-forming molecular moieties in a rigid way so that C_{60}–C_{60} interactions also contribute to the formation of ordered structures, rather than interfering with it. To this end, a series of shape-persistent molecules were designed in which C_{60} and OF hybrids were linked through a rigid spiro linkage at the 9 position of the fluorene unit, thus forming a cyclopropane ring on the C_{60} sphere (Scheme 1). The fluorene trimer was chosen and, to start with, C_{60} was attached onto the center of fluorene unit. The alkyl chains on the other two fluorene units ensured the solubility of these compounds and they could also be used to tune the fine structure of the self-assembled crystals. Three different alkyl-chain lengths were used: 1) *n*-butyl (butyl-OF-C_{60}); 2) *n*-octyl (octyl-OF-C_{60}); and 3) *n*-dodecanyl (dodecanyl-OF-C_{60}). Notably, it was also possible to change the alkyl chains to oligo(ethylene glycol) tails to impart water solubility or to perfluorinated alkyl chains to impart fluorophilic interactions and surface activity onto the material so as to diversify their final applications, which are topics of interest that are currently under investigation in our group.

The synthesis of the OF-C_{60} dyads was conveniently achieved in two steps from readily available starting materials (Scheme 1 A). The synthesis of compounds **1** and **2a**–**2c** has been well documented in the literature.[20] First, Suzuki–Miyaura cross-couplings reactions were used to construct the oligofluorene in 90% yield by using $[Pd(PPh_3)_4]$ as the catalyst.[20c,d] The final dyads were obtained through a typical diazo-addition reaction, as developed by Wudl and co-workers.[21] Ketones **3a**–**3c** were first reacted with *p*-toluenesulfonylhydrazide to afford hydrazones **4a**–**4c**. Without further purification, the hydrazones were treated with sodium methoxide in pyridine to generate nitrene in situ, which subsequently reacted with C_{60} at reflux in *o*-dichlorobenzene to afford the OF-C_{60} dyads in about 35% yield. The products were obtained as crystalline brown powders that were readily soluble in common organic solvents, such as toluene, $CHCl_3$, THF, and CH_2Cl_2. As expected, with increasing alkyl-chain length, the dyads exhibited much higher solubility in common organic solvents. Finally, the dyads were fully characterized by ^{1}H NMR (Figure 1 and the Supporting Information, Figures S4 and S8), ^{13}C NMR (the Supporting Information, Figures S1, S5, and S9), and FTIR spectroscopy (the Supporting Information, Figures S2, S6, and S10) and by MALDI-TOF mass spectrometry (the Supporting Information, Figures S3, S7, and S11) to establish their chemical structure and purity.

The success of the cross-coupling reaction in the first step was evidenced by the much increased fluorescence and larger R_f value of compound **3** in the TLC analysis (R_f=0.71 in toluene, versus 0.40 for compound **1**). After the attachment of C_{60}, the fluorescence was significantly quenched and the R_f value changed from 0.10 to 0.20 (cyclohexane/toluene, 10:1 v/v). In the ^{1}H NMR spectra (Figure 1), the singlet that was attributed to the protons at the 1 and 1′ positions of the central fluorene moiety exhibited a significant downfield shift from δ=8.04 ppm in compound **3a** to δ=9.30 ppm in butyl-OF-C_{60}, owing to the deshielding effect of the adjacent C_{60} cage. The signals from other protons on the central fluorene moiety also shifted downfield to some extent, whereas the signals that corresponded to the protons on the peripheral fluorene units remained essentially unaffected. In the ^{13}C NMR spectra (see the Supporting Information, Figure S1), 14 new peaks appeared from δ=148 to 140 ppm (in the Csp^2 region) and a new peak appeared at δ=78.95 ppm, which corresponded to the Csp^3 atoms in C_{60}. In the FTIR spectra (see the Supporting Information, Figure S2), the strong carbonyl absorption at 1720 cm^{-1} in compound **3a** disappeared in butyl-OF-C_{60} and a new sharp peak appeared at about 527 cm^{-1}, which was characteristic of the C–C vibration of C_{60}.[22] The MALDI-TOF mass spectra (see the Supporting Information, Figure S3) further confirmed the structures; the observed molecular-ion peaks had *m*/*z* values that matched well with those of the calculated monoisotopic masses. All of this evidence clearly confirmed that the chemical structure of OF-C_{60} was as proposed.

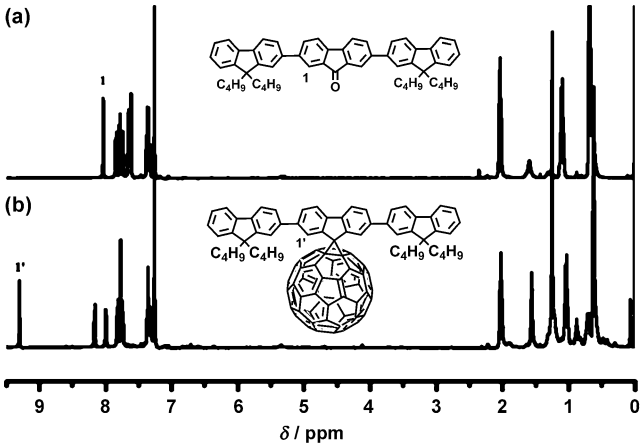

Figure 1. ^{1}H NMR spectra of compounds **3a** (a) and **5a** (b).

Crystal Morphologies and Structures

Excluding alkyl chains, the main scaffold of the dyads has a lateral dimension of about 2.1–2.3 nm, a width of about 1.1 nm, and a thickness of about 1.0 nm (Scheme 1 C). The contour lengths of butyl, octyl, and dodecanyl side-chains, as shown in Scheme 1 C, are about 0.53, 1.00, and 1.52 nm, respectively, assuming the formation of an extended chain with an all-*trans* conformation. Overall, the dyads are shape-persistent with a rigid conformation, except for the alkyl side-chains. The close packing of such rigid molecules is quite intriguing in its own right. The self-assembly was performed by the slow evaporation of a poor solvent, Et_2O, into a dilute solution of the dyads in $CHCl_3$ to induce crystallization. Small crystals could be easily grown in regular shapes (see below). The crystals were either deposited directly onto copper grids for TEM studies or collected as

a powdered sample for WAXD. The structure and molecular-packing scheme were illustrated based on combined results from TEM and WAXD. The crystal-structure determination for a representative example, butyl-OF-C_{60}, is discussed below. The results of the other two compounds were quite similar and are summarized in the Supporting Information.

Figure 2 shows a 1D WAXD pattern of butyl-OF-C_{60}. All of the diffraction peaks are assigned in the Supporting Information, Table S1. The *d* spacings of the first five strong diffraction peaks are 2.08 nm ($2\theta = 4.24°$), 2.01 nm ($2\theta = 4.40°$), 1.85 nm ($2\theta = 4.78°$), 1.73 nm ($2\theta = 5.10°$), and 1.27 nm ($2\theta = 6.96°$), respectively. Because the 1D WAXD pattern does not provide information on the dimensionality of the diffractions, 2D diffraction patterns are needed to determine the crystallographic unit-cell dimensions and symmetry.[23]

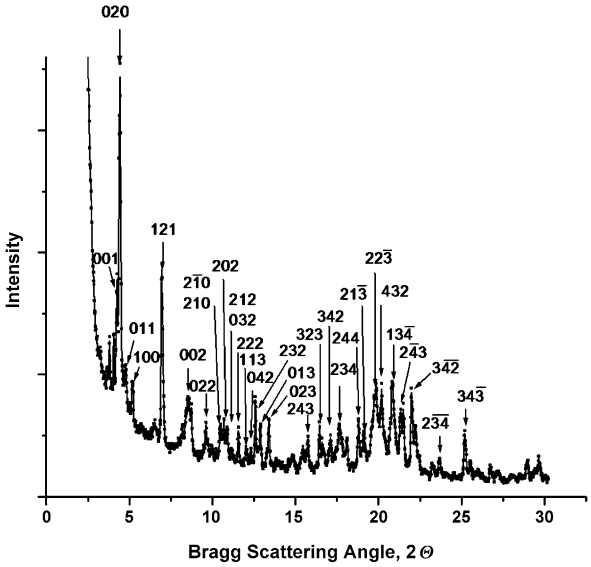

Figure 2. 1D WAXD pattern of a powdered sample of butyl-OF-C_{60}.

Figure 3a shows a bright-field TEM image of the single-crystal morphology of butyl-OF-C_{60}. The single crystal is in a parallelogram shape with a non-perpendicular angular relationship between both boundary sets. This shape of this single crystal hints at a unit-cell structure with relatively low symmetry, most likely monoclinic or triclinic. Figure 3b shows an ED pattern along the [010] direction, as taken from the single crystal in Figure 3a. The ED pattern along the [011] direction (Figure 3c) was obtained by rotating the crystal 28° clockwise around the a^* axis (as indicated in the Figure). An identical ED pattern along the [01$\bar{1}$] direction (Figure 3d) was obtained by rotating the crystal 28° counterclockwise around the same a^* axis. Because both the [011] and [01$\bar{1}$] directions are symmetric around the b^* axis (and, thus, also symmetric in the unit cell in real space), the unit cell can be determined to be monoclinic. In the ED pattern of Figure 3b, the electron beam is parallel to the *b* axis and, thus, the angle (β^*) between the a^* and c^* axes could be determined to be 112°. Selected-area ED patterns (Figure 3b–d) indicate that this lattice does not show systematic extinction. Thus, the space group is assigned to be *P2*. In summary, the butyl-OF-C_{60} crystal structure forms a monoclinic unit cell with $a = 1.86$, $b = 3.96$, $c = 2.24$ nm; $\alpha = \gamma = 90°$, $\beta = 68°$. The calculated density of a cell that contained eight butyl-OF-C_{60} molecules was 1.24 g cm^{-3}, which agreed very well with the measured density of 1.22 g cm^{-3}.

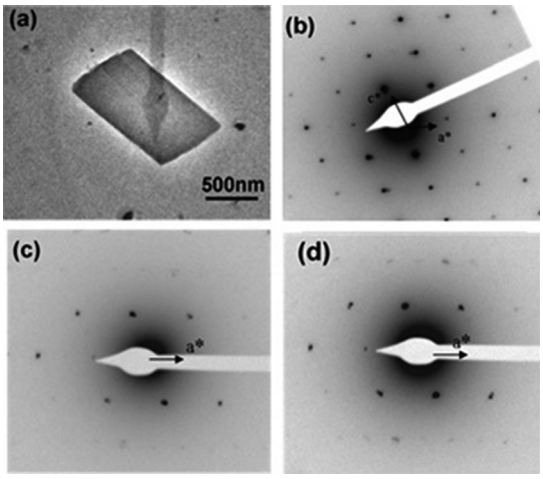

Figure 3. TEM bright-field morphology of a) single-crystal butyl-OF-C_{60} and the selected-area ED patterns along the [010] (b), [011] (c), and [01$\bar{1}$] (d) directions of the single crystal.

Next, the molecular-packing model of butyl-OF-C_{60} was constructed by using the Cerius^2 modeling software (Figure 4a–c). Figure 4a shows the projection of a butyl-OF-C_{60} single-crystal cell on the *ab* plane. The projection of a butyl-OF-C_{60} single-crystal cell on the *bc* plane is shown in Figure 4b and the projection of a butyl-OF-C_{60} single-crystal cell on the *ac* plane is shown in Figure 4c. Figure 4a,b shows the layered packing of the molecules, in which bi-layered C_{60} moieties are packed alternatively with the OF

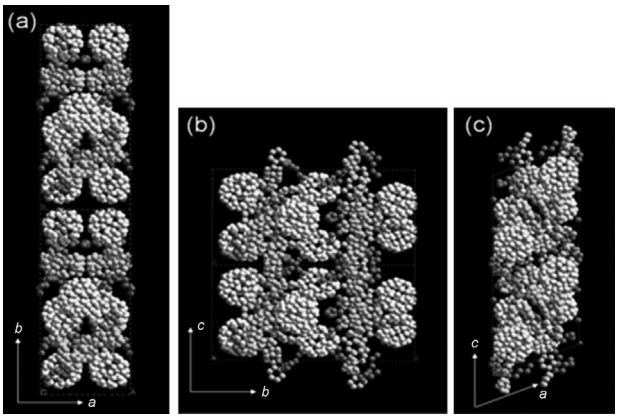

Figure 4. Molecular-packing model of butyl-OF-C_{60} single crystals, as obtained by using the Cerius^2 simulation program: projections of the single crystal on the *ab* plane (a), *bc* plane (b), and *ac* plane (c).

layers along the *b* axis. As shown in Figure 4c, that the π–π stacking of OF moieties should not be dominant, owing to the distinct differences between the OF and C_{60} moieties in terms of their volume and shape. The calculated electron-diffraction patterns along the [010], [011], and [01$\bar{1}$] directions, as obtained by using the Cerius[2] simulation program, are shown in Figure 5a–c, respectively. The sets of (001),

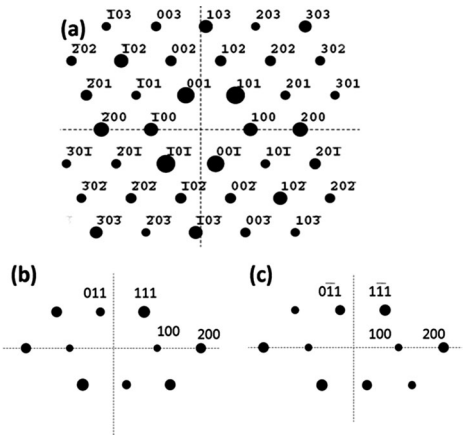

Figure 5. Calculated ED pattern along the a) [010], b) [011], c) [01$\bar{1}$] directions, as obtained by using the Cerius[2] simulation program.

(100), (101), (102), (103), (202), (203), and other electron diffractions in the calculated ED pattern along the [010] direction are unambiguously assigned in Figure 5a, and all of these simulated ED patterns fit very well with the experimental results (Figure 3b–d). Similarly, the crystal structures of octyl-OF-C_{60} and dodecanyl-OF-C_{60} were also determined. The octyl-OF-C_{60} unit cell is also monoclinic (a = 2.21, b = 4.06, c = 1.81 nm; $\alpha = \gamma = 90°$, $\beta = 75.5°$; space group *C2m*) and the dodecanyl-OF-C_{60} unit cell has a triclinic structure (a = 1.82, b = 4.35, c = 2.26 nm; $\alpha = 93.1°$, $\beta = 94.5°$, $\gamma = 92.7°$; space group *P1*). The constructed molecular-packing schemes are shown in Figure 6 and Figure 7 (see the Supporting Information for WAXD and ED results). The simulated electron-diffraction patterns (see the Supporting Information, Figures S14 and S17) matched well with the experimental results, which verified the proposed molecular-packing schemes in the crystals.

It is evident that all of the three crystal structures exhibit a similar molecular packing scheme, in which the C_{60} and OF moieties are arranged in alternating layers. This result can be understood from their inequivalent shapes and interactions. Although the major interactions of these two units are both π–π interactions in nature, the interactions between C_{60} moieties are isotropic and those between OF moieties are anisotropic. Owing to the packing constraints imposed by the spherical shape of C_{60} and the rod shape of OF, the final packing maximizes the contact between C_{60}s but not between OFs. As a result, the interactions between OF moieties are just sufficient to hold the OF units together. When the alkyl side-chains are shorter, as in the case of butyl-OF-C_{60}, the C_{60} spheres can interact by intercalating

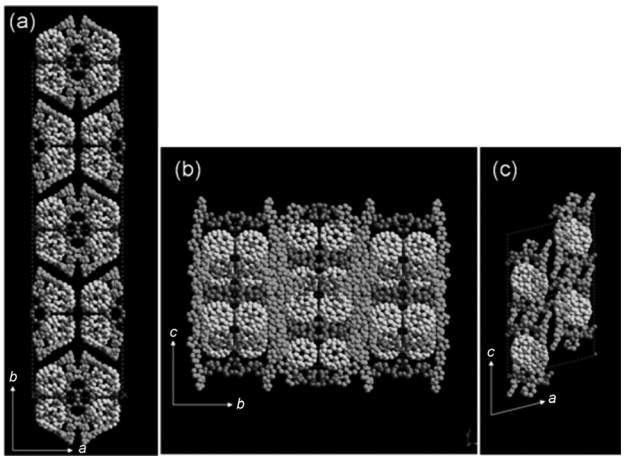

Figure 6. Molecular-packing model of octyl-OF-C_{60} single crystals, as established by using the Cerius[2] simulation program: projections of the single crystal on the *ab* plane (a), *bc* plane (b), and *ac* plane (c).

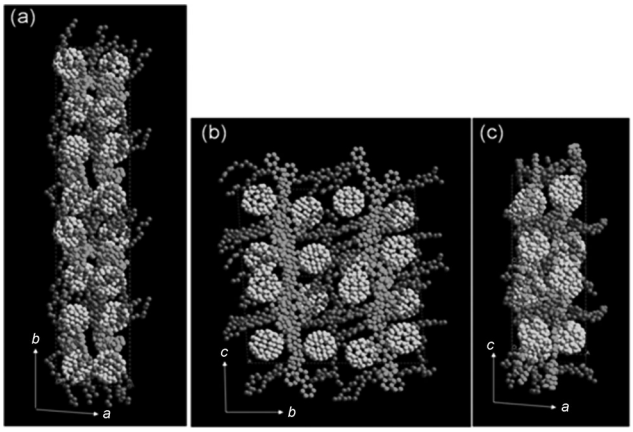

Figure 7. Molecular-packing model of dodecanyl-OF-C_{60} single crystals, as established by using the Cerius[2] simulation program: projections of the single crystal on the *ab* plane (a), *bc* plane (b), and *ac* plane (c).

with each other and pack more closely together. With increasing side-chain length, the *b* dimension increases from 3.96 to 4.06 nm and further to 4.35 nm. The alkyl chains fill in the gaps between the C_{60} spheres, thereby leaving more space for the close packing of the rod-like planar OF moieties. Meanwhile, the interactions between the C_{60} spheres decrease, because their content is diluted by the presence of the alkyl groups. Notably, although the molecular-packing pattern is preserved, the detailed unit symmetry is changed from monoclinic to triclinic. Whereas long alkyl chains increase the solubility and processability of the material, they also "dilute" the effective content of the electro-active components in the molecule, which may be detrimental to the final electronic properties. The best electronic properties are expected from those structures with shorter side-chains, in which there is an ordered structure with sufficiently good contact between the electro-active components in the bulk state.

Optical and Electronic Properties

The optical and electronic properties of dyads of OF-C_{60} were studied by UV/Vis absorption spectroscopy, fluorescence spectroscopy, and cyclic voltammetry. A fluorene trimer (Scheme 1B), was chosen as a control compound instead of precursor **3**, because the ketone group in compound **3** is known to have a significant effect on the optical and electronic properties of the oligofluorene unit.[24] In dilute solutions, these compounds exhibit single-molecular behavior.[25] Because they possess exactly the same chromophore, their absorption profiles and fluorescence profiles are essentially identical (see the Supporting Information, Figures S18 and S19). Therefore, only butyl-OF-C_{60} is discussed below as a representative example.

The steady-state UV/Vis absorption spectra were recorded in toluene at room temperature. Figure 8a shows the absorption spectra of C_{60}, butyl-OF-C_{60}, OF, and an OF/C_{60} blend. The absorption peaks at about 330 nm and 430 nm are typical fingerprints of C_{60} monoadducts (methanofullerene),[14a,26] whereas the peaks at about 350 nm are characteristic of the oligofluorene unit.[24a] The absorption profile of butyl-OF-C_{60} around 350 nm is broadened as compared to that of OF and the OF/C_{60} blend, suggesting an electronic perturbation between the two individual chromophores (OF and C_{60}) in their ground states.[27]

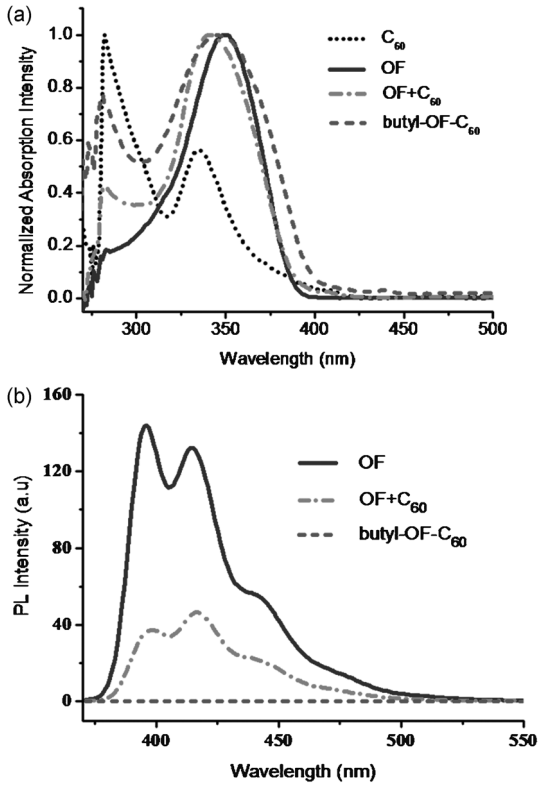

Figure 8. a) Steady-state UV/Vis absorption spectra of C_{60}, butyl-OF-C_{60}, OF, and an OF/C_{60} blend; b) fluorescence spectra of OF, an OF/C_{60} blend, and butyl-OF-C_{60}.

The fluorescence emission spectra of the OF-C_{60} dyads were also recorded in toluene at room temperature. The excitation wavelength was 350 nm, which was the absorption maximum for the OF-C_{60} dyads. In all of the samples, quantitative quenching of the fluorescent emission was observed, which was clear evidence for efficient energy transfer from OF to C_{60}.[14b,27b,28] For reference, the fluorescence spectra of OF and an OF/C_{60} blend were also recorded in toluene and compared to that of butyl-OF-C_{60} (Figure 8b). The spectrum of pristine oligofluorene showed two emission peaks at 395 nm and 415 nm, whilst that of the OF/C_{60} blend showed partial fluorescence quenching at an identical concentration of OF, but complete fluorescence quenching was only observed in the case of butyl-OF-C_{60}, in which where the C_{60} and OF were covalently linked and proximal to one another. The interactions between the exited states of oligofluorene and fullerene are believed to take place with efficient energy transfer from the singlet-excited-state energy of the oligofluorene segment to the fullerene core. Charge separation may occur during the excitation process.[27a,b]

The electronic properties of C_{60}, OF, and the OF-C_{60} dyads were studied by using cyclic voltammetry; the voltammograms are shown in Figure 9 and the results are summarized in Table 1. In general, the OF-C_{60} dyads show similar electrochemical behavior to its two components. In the cathodic region, no reduction peak was observed for OF, whereas C_{60} displayed four typical reduction peaks and the OF-C_{60} dyads showed the typical voltammogram for a methanofullerene derivative.[27b,29] For butyl-OF-C_{60}, the first reduction peak appears at around −1.07 V versus Fc/Fc^+ and is fully reversible. In contrast, the second reduction peak appears at −1.45 V versus Fc/Fc^+ and is irreversible. Both of these reduction potentials are shifted to more-negative values compared to that of C_{60}, because the saturation of a double bond on the C_{60} surface cause a partial loss of "conjugation".[27a,29a,30] The third redox wave is new compared with the spectrum of C_{60}, which is associated with the change of electronic structure in butyl-OF-C_{60} upon conjuga-

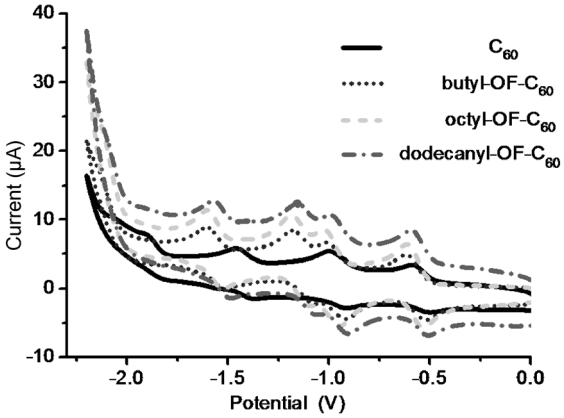

Figure 9. Cyclic voltammograms of C_{60}, butyl-OF-C_{60} (**5a**), octyl-OF-C_{60} (**5b**), and dodecanyl-OF-C_{60} (**5c**).

Table 1. Cyclic voltammetry data, HOMO and LUMO levels, and Eg^{CV} and Eg^{opt} of C_{60}, OF, and the OF-C_{60} dyads.

Compound	$E^1_{1/2,red}$[a] [V]	$E^2_{1/2,red}$ [V]	$E^3_{1/2,red}$ [V]	$E^4_{1/2,red}$ [V]	$E^5_{1/2,red}$ [V]	$E_{1/2,ox}$ [V]	HOMO[b] [eV]	LUMO [eV]	Eg^{CV}[e] [eV]	Eg^{opt}[f] [eV]
C_{60}	−1.03	−1.44	–	−1.90	−2.21	–	–	−4.07[c]	–	–
OF	–	–	–	–	–	0.80	−5.90	−2.72[d]	3.18	3.18
butyl-OF-C_{60}	−1.07	−1.45	−1.76	−2.07	−2.40	0.88	−5.98	−4.03[d]	1.95	3.08
octyl-OF-C_{60}	−1.05	−1.45	−1.63	−2.05	−2.40	0.90	−6.00	−4.05[d]	1.95	3.08
dodecanyl-OF-C_{60}	−1.06	−1.46	−1.64	−2.06	−2.39	0.89	−5.99	−4.04[d]	1.95	3.10

[a] Reduction/oxidation potentials (versus Fc/Fc^+) for each couple are calculated according to $E_{1/2}=(E_{pc}+E_{pa})/2$, where E_{pc} is the cathodic peak potential and E_{pa} is the anodic peak potential. [b] HOMO energy levels were calculated according to $E_{HOMO}=(-E_{1/2,ox}-5.10)$. [c] LUMO energy levels were calculated according to $E_{LUMO}=(-E_{1/2,red}-5.10)$ or [d] from the optical energy gap, according to $E_{LUMO}=E_{HOMO}+Eg^{opt}$. [e] Calculated according to $Eg^{CV}=E_{LUMO}-E_{HOMO}$. [f] Calculated according to $Eg^{opt}=1240/\lambda$, where λ (in nm) is the onset absorption wavelength.

tion.[27b,29,31] It has been reported that a bond in the cyclopropane ring of methanofullerene derivatives may break upon the second reduction, which has been referred to as the retro-Bingel reaction.[29b,31,32] The fourth and fifth redox waves are also shifted to more-negative values compared to those of C_{60}. All of the five reduction peaks are due to the fullerene core, so the energy-level profiles of C_{60} and OF remain essentially unchanged. In the anodic region, OF shows two reversible redox waves at 0.80 V and 1.13 V versus Fc/Fc^+ and butyl-OF-C_{60} shows one irreversible redox wave at 0.88 V versus Fc/Fc^+, which is shifted to more-positive potential values compared to the first redox wave of OF. This result is caused by the electronic interactions between the electron-donating π-conjugated oligofluorene and the electron-accepting C_{60}.[27a,c,30b]

The optical energy gaps of the OF-C_{60} dyads and OF (Table 1) were calculated from the onset of the UV/Vis absorption, according to the equation $Eg=1240/\lambda$, where λ (in nm) is the onset absorption wavelength.[33] The optical energy gaps of the OF-C_{60} dyads were attributed to the oligofluorene moiety, which was lower than that of OF, thus indicating an increase in the conjugation of the OF moieties when attached to C_{60}. The HOMO and LUMO levels of the OF-C_{60} dyads were calculated from the half-wave potentials by assuming that the energy level of Fc/Fc^+ was −5.10 eV below the vacuum level.[33,34] The HOMO levels of the OF-C_{60} dyads are similar to the HOMO level of OF and the LUMO levels of OF-C_{60} dyads are similar to that of C_{60}, which means that the HOMO of the OF-C_{60} dyads is located on the OF moieties and the LUMO is located on the C_{60} moieties. The HOMO levels of the OF-C_{60} dyads are slightly lower than that of OF, whereas the LUMO levels of the OF-C_{60} dyads are higher than that of C_{60}, owing to electronic communication between the electron-donating π-conjugated system and the electron-accepting C_{60} moiety.[35] The electrochemical energy gaps (Eg^{CV}, $Eg^{CV}=E_{LUMO}-E_{HOMO}$) in the OF-$C_{60}$ dyads are much smaller than the optical energy levels (Eg^{opt}), because the electrochemical energy gaps are the difference in energy levels between the LUMO of the C_{60} moieties and the HOMO of the OF moieties.

Conclusions

In summary, a series of sphere–rod shape amphiphiles has been designed and synthesized based on C_{60} and oligofluorene (OF). The OF was functionalized with C_{60} at the 9 position of its central fluorene unit through a rigid spiro linkage to form C_{60}–C_{60} interactions that contributed to the formation of an ordered structure. The conjugates contained three alkyl chains of different lengths to tune their solubility and solid-state structure. The butyl-OF-C_{60} conjugate formed a monoclinic unit cell ($a=1.86$, $b=3.96$, $c=2.24$ nm; $\alpha=\gamma=90°$, $\beta=68°$; space group *P2*), the octyl-OF-C_{60} also formed a monoclinic unit cell ($a=2.21$, $b=4.06$, $c=1.81$ nm; $\alpha=\gamma=90°$, $\beta=75.5°$; space group *C2m*), and dodecanyl-OF-C_{60} formed a triclinic structure ($a=1.82$, $b=4.35$, $c=2.26$ nm; $\alpha=93.1°$, $\beta=94.5°$, $\gamma=92.7°$; space group *P1*). In the crystals, C_{60} and OF form an alternating packing structure due to the inequivalence in shape. As shown by UV/Vis absorption and fluorescence spectroscopy, the OF-C_{60} conjugates exhibit an efficient energy transfer from OF to C_{60}. These new structures will shed light on the structure–property relationships and their device performance, such as in organic field-effect transistors and bulk heterojunction solar cells. These results also have general implications in the understanding of the self-assembly of π-conjugated materials.

Experimental Section

Chemicals and Solvents

[60]Fullerene (MTR Ltd., >99.5%), [$Pd(PPh_3)_4$] (J&K, 99.9%), *p*-toluenesulfonyl hydrazide (J&K, 97%), anhydrous sodium carbonate (SINOPHARM, ACS grade), sodium methoxide (SINOPHARM, ACS grade), THF (SINOPHARM, ACS grade), MeOH (Fisher Scientific, reagent grade), CS_2 (Aldrich ACS grade), petroleum ether (SINOPHARM, ACS grade), and cyclohexane (SINOPHARM, ACS grade) were used as received. Toluene (SINOPHARM, ACS grade) was purified by distillation from CaH_2 and then sodium before it was stored over poly(styryl)lithium. Pyridine (SINOPHARM, ACS grade) was purified by distillation from KOH. *o*-Dichlorobenzene (o-DCB, SINOPHARM, ACS grade) was purified by distillation from CaH_2. 2,7-Dibromofluoren-9-one, 9,9-dialkyl-2-bromofluorene, and 9,9-dialkylfluoreneyl-2-boronic acid were prepared according to literature procedures.[20]

Instruments

All ^1H and ^{13}C NMR spectra were acquired at RT in $CDCl_3$ (Aldrich, 99.8% D) on a Varian Mercury 500 NMR spectrometer that was operat-

ing at 500 MHz and 125 MHz, respectively. The ^{1}H NMR spectra were referenced to residual protons impurities in the $CDCl_3$ solvent ($\delta =$ 7.27 ppm) and the ^{13}C NMR spectra were referenced to $^{13}CDCl_3$ ($\delta =$ 77.00 ppm). The coupling constants (J) are reported in Hertz (Hz) and the NMR splitting patterns are characterized as follows: s singlet, d doubled, t triplet, and m multiplet. Fourier-transform infrared (FTIR) spectra were recorded on a Nicolet Magna-IR 550 FTIR spectrometer in the range 400–4000 cm^{-1} by making KBr pellets. The resolution was 4 cm^{-1} and the spectra were averages of 32 scans.

Matrix-assisted laser-desorption/ionization time-of-flight (MALDI-TOF) mass spectra were recorded on a KratosAximaCFR plus spectrometer (Shimadzu Biotech, Manchester, UK) with a 337 nm nitrogen laser and an accelerating voltage of 20 kV. The homemade sample support was attached onto the MALDI plate by using a double-sided tap before sample deposition. The sample solution (1 μL) was deposited onto the traditional MALDI plate or the new sample support. The matrix, 2,5-dihydroxybenzoic acid (DHB), was dissolved in water that contained 50% (v/v) MeCN and 0.1% (v/v) trifluoroacetic acid (TFA) at a concentration of 10 mg mL^{-1}. After drying in air, 1 μL of the matrix solution was deposited onto the dried analyte spot for MALDI analysis. Mass spectra in positive-ion mode were measured in both linear and reflectron modes. Data analyses were conducted with the Kompact software.

1D WAXD patterns were obtained on a Rigaku Multiflex 2kW Automated Diffractometer by using $Cu_{K\alpha}$ radiation (0.1542 nm). The samples were scanned in over the range $2\theta = 2$–30° at a rate of 1° min^{-1}. TEM experiments were performed on a Philips Tecnai 12 at an accelerating voltage of 120 kV. Selected-area electron diffraction (SAED) patterns were obtained by using a TEM tilting stage to determine the crystal-structure parameters. The d spacings were calibrated by using a TlCl standard. Computer molecular modeling and the calculated electron-diffraction patterns were determined by using the Cerius^2 package of Accelrys. The basic unit-cell parameters, as determined by using the crystallographic experimental data from the 1D WAXD and SAED experiments, were used as a reference in building the molecular packing scheme within the crystallographic unit cells.

UV/Vis spectra were measured on a CARY 100 UV/Vis spectrophotometer. The samples were prepared in toluene at a concentration of 5×10^{-5} M and the spectra were recorded between 200 nm and 600 nm. The fluorescence spectra were measured on a CARY Eclipse Fluorescence spectrophotometer after excitation at the maximum absorption wavelength of the compounds.

Cyclic voltammograms were recorded on a potentiostant/galvanostat that was equipped with GPES software for Windows (version 4.8). All experiments were performed at RT in *o*-DCB/MeCN (4:1) that contained tetrabutylammonium perchlorate as the supporting electrolyte, with glassy carbon as the working electrode, platinum wire as the counter electrode, and Ag/AgCl as the reference electrode at a scan rate of 100 mV s^{-1}. Potentials were referenced to the Fc/Fc^+ (ferrocene/ferrocenium, Alfa-Aesar) couple.

Typical Synthetic Procedures

9,9,9″,9″-Tetra(*n*-butyl)-9′-one-terfluorene (3a): A mixture of 2,7-dibromofluoren-9-one (**1**, 0.44 g, 1.3 mmol), 9,9-di(*n*-butylfluoreneyl)-2-boronic acid (**2a**, 1.00 g, 3.12 mmol), $[Pd(PPh_3)_4]$ (36 mg, 0.031 mmol), an aqueous solution of Na_2CO_3 (2.0 M, 8 mL, 16 mmol), and toluene (20 mL) was stirred at 90 °C for 2 days. After cooling to RT, petroleum ether (200 mL) was added to the reaction mixture. The organic portion was separated and washed with brine before drying over anhydrous $MgSO_4$. The solvent was evaporated off and the solid residues were recrystallized from EtOH to afford compound **3a** as yellow solids (0.87 g). Yield: 92%; ^{1}H NMR (500 MHz, $CDCl_3$): $\delta = 8.04$ (d, $J = 1.7$ Hz, 2H), 7.84 (dd, $J = 7.7$, 1.8 Hz, 2H), 7.79 (d, $J = 7.8$ Hz, 2H), 7.77–7.72 (m, 2H), 7.69–7.59 (m, 6H), 7.41–7.31 (m, 6H), 2.04 (t, $J = 8.3$ Hz, 8H), 1.13–1.08 (m, 8H), 0.74–0.56 ppm (m, 20H); ^{13}C NMR ($CDCl_3$, 125 MHz): $\delta = 194.91$, 152.32, 151.70, 143.65, 143.35, 141.85, 141.23, 139.24, 135.93, 134.09, 127.98, 127.54, 126.32, 123.78, 123.63, 121.69, 121.46, 120.78, 120.30, 55.88, 40.96, 26.69, 23.76, 14.53 ppm; FTIR (KBr): $\tilde{\nu} = 2930$, 1720 (C=O), 1450, 1120, 821, 741 cm^{-1}; MS (MALDI-TOF): m/z calcd for $C_{55}H_{56}O$: 733.0; found: 732.5.

9,9,9″,9″-Tetra(*n*-butyl)-9′-(*p*-tosylhydrazone)-terfluorene (4a): A mixture of 9,9,9″,9″-tetra(*n*-butyl)-9′-one-terfluorene (**3a**, 0.66 g, 0.9 mmol), *p*-toluenesulfonylhydrazide (0.20 g, 1.08 mmol), and THF (70 mL) with a catalytic amount of HCl was stirred at reflux for 7 h. After cooling to RT, the solvent were evaporated off and the solid residue was washed with MeOH to afford a yellow solid (0.73 g, 89% yield). The sample was directly subject to next step without further purification.

9,9,9″,9″-Tetra(*n*-butyl)-9′-fullerenyl-terfluorene (butyl-OF-C_{60}, 5a): A mixture of 9,9,9″,9″-tetra(*n*-butyl)-9′-(*p*-tosylhydrazone)-terfluorene (**4a**, 0.72 g, 0.8 mmol), sodium methoxide (0.065 g, 1.2 mmol), and dry degassed pyridine (50 mL) was stirred under a nitrogen atmosphere at RT for 30 min. To the mixture was added a solution of C_{60} (0.29 g, 0.4 mmol) in degassed o-DCB (200 mL) and the homogeneous mixture was stirred at 80 °C under a nitrogen atmosphere for 24 h. After heating at reflux for a further 24 h, the mixture was concentrated under vacuum to 100 mL, loaded onto the top of a silica-gel column, and eluted first with cyclohexane/carbon disulfide (10:1 v/v) followed by cyclohexane/toluene (10:1 v/v). The first fraction, which contained unreacted C_{60}, was collected. After the elution of an intermediate fraction, a fraction that contained butyl-OF-C_{60} was collected. After evaporation, butyl-OF-C_{60} was obtained as a shiny black crystalline solid (0.20 g). Yield: 35%; ^{1}H NMR ($CDCl_3$, 500 MHz): $\delta = 9.29$ (d, $J = 1.5$ Hz, 2H), 8.16 (d, $J = 7.9$ Hz, 2H), 7.98 (dd, $J = 7.9$, 1.5 Hz, 2H), 7.85–7.79 (m, 2H), 7.78–7.71 (m, 6H), 7.30–7.37 (m, 6H), 2.10–1.90 (m, 8H), 1.02–1.06 (m, 8H), 0.58–0.71 ppm (m, 20H); ^{13}C NMR ($CDCl_3$, 125 MHz): $\delta = 152.21$, 151.34, 148.51, 146.16, 145.92, 145.39, 145.31, 144.53, 144.04,143.95, 143.83, 143.76, 142.84, 141.98, 141.65, 141.36, 141.19, 140.42, 140.21, 139.79, 128.13, 127.79, 127.47, 126.49, 124.63, 123.44, 121.88, 121.08, 120.85, 120.43, 77.95, 55.61, 41.20, 26.84, 24.07, 14.68 ppm; FTIR (KBr): $\tilde{\nu} = 2920$, 1450, 1090, 828, 739, 527 cm^{-1}; MS (MALDI-TOF): m/z calcd for $C_{115}H_{56}$: 1437.7; found: 1437.3.

Sample Preparation for Crystal-Structure Determination

Milligrams of the materials were dissolved in a test tube to afford a saturated solution (about 1 wt.%) in $CHCl_3$. Then, the test tube was covered with paper and placed in a closed chamber that was saturated with Et_2O. The single crystals were typically grown within several hours as the Et_2O slowly evaporated into the sample solution. A drop of the solution that contained the single crystals was deposited onto the carbon-coated copper grids for the TEM experiments. The powders were collected by filtration for wide-angle X-ray diffraction experiments.

Acknowledgements

This work was supported by the Natural Science Foundation of Shanghai (10ZR1407600), the NSF (DMR-0906898), and by the Joint-Hope Education Foundation. The authors thank Mr. Gengxin Liu and Mr. Hao Sun for their helpful discussions.

[1] a) S. C. Glotzer, M. A. Horsch, C. R. Iacovella, Z. L. Zhang, E. R. Chan, X. Zhang, *Curr. Opin. Colloid Interface Sci.* **2005**, *10*, 287–295; b) Z. L. Zhang, M. A. Horsch, M. H. Lamm, S. C. Glotzer, *Nano Lett.* **2003**, *3*, 1341–1346; c) P. van Rijn, D. Janeliunas, A. M. A. Brizard, M. C. A. Atuart, R. Eelkema, J. H. Esch, *Chem. Eur. J.* **2010**, *16*, 13417–13428; d) J. H. Ryu, D. J. Hong, M. Lee, *Chem. Commun.* **2008**, 1043–1054.

[2] a) W. B. Zhang, Y. W. Li, X. P. Li, X. H. Dong, X. F. Yu, C. L. Wang, C. Wesdemiotis, R. P. Quirk, S. Z. D. Cheng, *Macromolecules* **2011**, *44*, 2589–2596; b) R. W. Date, D. W. Bruce, *J. Am. Chem. Soc.* **2003**, *125*, 9012–9013; c) X. Zhang, E. R. Chan, S. C. Glotzer, *J. Chem. Phys.* **2005**, *123*, 184718; d) C. R. Iacovella, M. A. Horsch, Z. L. Zhang, S. C. Glotzer, *Langmuir* **2005**, *21*, 9488–9494.

[3] a) I. C. Reynhout, J. J. L. M. Cornelissen, R. J. M. Nolte, *Acc. Chem. Res.* **2009**, *42*, 681–692; b) X. F. Yu, S. Zhong, X. P. Li, Y. F. Tu, S. G. Yang, R. M. V. Horn, C. Y. Ni, D. J. Pochan, R. P. Quirk, C. Wesdemiotis, W. B. Zhang, S. Z. D. Cheng, *J. Am. Chem. Soc.* **2010**, *132*, 16741–16744; c) K. S. Kumar, A. Patnaik, *Langmuir* **2011**, *27*, 11017–11025.

[4] H. J. Sun, Y. F. Tu, C. L. Wang, R. M. V. Horn, C. C. Tsai, M. J. Graham, B. Sun, B. Lotz, W. B. Zhang, S. Z. D. Cheng, *J. Mater. Chem.* **2011**, *21*, 14240–14247.

[5] a) F. Giacalone, N. Martin, *Chem. Rev.* **2006**, *106*, 5136–5190; b) Y. Chen, M. E. E. Khouly, X. D. Zhuang, N. He, Y. Araki, Y. Lin, O. Ito, *Chem. Eur. J.* **2007**, *13*, 1709–1714; c) A. Gégout, J. L. Delgado, J. F. Nierengarten, B. D. Nicot, A. Listorti, C. Chiorboli, *New J. Chem.* **2009**, *33*, 2174–2182; d) F. Langa, M. J. G. Escalonilla, J. M. Rueff, T. M. F. Duarte, J. F. Nierengarten, V. Palermo, P. Samori, Y. Rio, G. Accorsi, N. Armaroli, *Chem. Eur. J.* **2005**, *11*, 4405–4415.

[6] S. C. Glotzer, *Science* **2004**, *306*, 419–420.

[7] a) C. L. Wang, W. B. Zhang, R. M. V. Hom, Y. F. Tu, X. Gong, S. Z. D. Cheng, Y. M. Sun, M. H. Tong, J. Seo, B. B. Y. Hsu, A. J. Heeger, *Adv. Mater.* **2011**, *23*, 2951–2956; b) C. L. Wang, W.-B. Zhang, R. M. Van Horn, R. P. Kulkarni, H.-J. Sun, C.-H. Hsu, B. Lotz, X. Gong, S. Z. D. Cheng, *Adv. Energy Mater.* **2012**, *2*, 1375–1382.

[8] W. B. Zhang, Y. F. Tu, R. Ranjan, R. M. V. Horn, S. W. Leng, J. Wang, M. J. Polce, C. Wesdemiotis, R. P. Quirk, G. R. Wewkome, S. Z. D. Cheng, *Macromolecules* **2008**, *41*, 515–517.

[9] a) A. Cravino, *Polym. Int.* **2007**, *56*, 943–956; b) X. W. Chen, B. Gholamkhass, X. Han, G. Vamvounis, S. Holdcroft, *Macromol. Rapid Commun.* **2007**, *28*, 1792–1797; c) K. Kobata, J. Ogawa, S. S. Pandey, H. Oshima, T. Arai, T. Kato, N. Nishino, *Synth. Met.* **2007**, *157*, 311–317; d) F. Richard, C. Brochon, N. Leclerc, D. Eckhardt, T. Heiser, G. Hadziioannou, *Macromol. Rapid Commun.* **2008**, *29*, 885–891; e) B. de Boer, U. Stalmach, P. F. V. Hutten, C. Melzer, V. V. Krasnikov, G. Hadziioannou, *Polymer* **2001**, *42*, 9097–9109; f) U. Stalmach, B. D. Boer, C. Videlot, P. F. V. Hutten, G. Hadziioannou, *J. Am. Chem. Soc.* **2000**, *122*, 5464–5472.

[10] a) F. Ouhib, A. Khoukh, J. B. Ledeuil, H. Martinez, J. Desbrieres, C. D. Lartigau, *Macromolecules* **2008**, *41*, 9736–9743; b) Z. Tan, J. H. Hou, Y. J. He, E. Zhou, C. H. Yang, Y. F. Li, *Macromolecules* **2007**, *40*, 1868–1873; c) R. Bhosale, J. MíŠek, N. Sakai, S. Matile, *Chem. Soc. Rev.* **2010**, *39*, 138–149.

[11] a) J. U. Lee, A. Cirpan, T. Emrick, T. P. Russell, W. H. Jo, *J. Mater. Chem.* **2009**, *19*, 1483–1489; b) C. Yang, J. K. Lee, A. J. Heeger, F. Wudl, *J. Mater. Chem.* **2009**, *19*, 5416–5423; c) B. W. Boudouris, F. Molins, D. A. Blank, C. D. Frisbie, M. A. Hillmyer, *Macromolecules* **2009**, *42*, 4118–4126.

[12] J. F. Nierengarten, *Sol. Energy Mater. Sol. Cells* **2004**, *83*, 187–199.

[13] S. Barrau, T. Heiser, F. Richard, C. Brochon, C. Ngov, K. V. D. Wetering, G. Hadziioannou, D. V. Anokhin, A. Ivanov, *Macromolecules* **2008**, *41*, 2701–2710.

[14] a) J. L. Segura, N. Martin, D. M. Guldi, *Chem. Soc. Rev.* **2005**, *34*, 31–47; b) R. Gómez, J. L. Segura, *Tetrahedron* **2009**, *65*, 540–546; c) W. B. Zhang, W. H. Jin, X. H. Zhou, J. Pei, *Tetrahedron* **2007**, *63*, 2907–2914.

[15] J. Jo, C. Chi, S. Hoger, G. Wegner, D. Y. Yoon, *Chem. Eur. J.* **2004**, *10*, 2681–2688.

[16] T. M. Figueira-Duarte, A. Gegout, J. F. Nierengarten, *Chem. Commun.* **2007**, 109–119.

[17] a) J. A. Mikroyannidis, Y. J. Yu, S. H. Lee, J. I. Jin, *J. Polym. Sci. Part A* **2006**, *44*, 4494–4507; b) C. L. Chochos, P. K. Tsolakis, V. G. Gregoriou, J. K. Kallitsis, *Macromolecules* **2004**, *37*, 2502–2510; c) S. T. Lin, K. Fuchise, Y. Chen, R. Sakai, T. Satoh, T. Kakuchi, W. C. Chen, *Soft Matter* **2009**, *5*, 3761–3770; d) X. J. Zhang, H. K. Tian, Q. Liu, L. Wang, Y. H. Geng, F. S. Wang, *J. Org. Chem.* **2006**, *71*, 4332–4335.

[18] F. Caporossi, B. Floris, P. Galloni, E. Gatto, M. Venanzi, A. F. Mozzi, A. Urbani, K. M. Kadish, *Synth. Met.* **2009**, *159*, 1403–1408.

[19] C. van der Pol, M. R. Bryce, M. Wielopolski, C. Atienza-Castellanos, D. M. Guldi, S. Filippone, N. Martin, *J. Org. Chem.* **2007**, *72*, 6662–6671.

[20] a) L. Liu, W. Y. Wong, Y. W. Lam, W. Y. Tam, *Inorg. Chim. Acta* **2007**, *360*, 109–121; b) S. P. Dudek, M. Pouderoijen, R. Abbel, A. P. H. J. Schenning, E. W. Meijer, *J. Am. Chem. Soc.* **2005**, *127*, 11763–11768; c) Z. H. Li, M. S. Wong, Y. Tao, J. P. Lu, *Chem. Eur. J.* **2005**, *11*, 3285–3293; d) D. Katsis, Y. H. Geng, J. J. Ou, S. W. Culligan, A. Trajkovska, S. H. Chen, L. J. Rothberg, *Chem. Mater.* **2002**, *14*, 1332–1339.

[21] J. C. Hummelen, B. W. Knight, F. Lepeq, F. Wudl, *J. Org. Chem.* **1995**, *60*, 532–538.

[22] A. Hirsch, M. Brettreich, *Fullerenes: Chemistry and Reactions*, Wiley-VCH, Verlag, Weinheim, **2005**, pp. 34–39.

[23] a) S. W. Leng, B. Wex, L. H. Chan, M. J. Graham, S. Jin, A. J. Jing, K. U. Jeong, R. M. V. Horn, B. Sun, M. F. Zhu, B. R. Kaafarani, S. Z. D. Cheng, *J. Phys. Chem. B* **2009**, *113*, 5403–5411; b) X. K. Ren, B. Sun, C. C. Tsai, Y. F. Tu, S. W. Leng, K. X. Li, Z. Kang, R. M. V. Horn, X. P. Li, M. F. Zhu, C. Wesdemiotis, W. B. Zhang, S. Z. D. Cheng, *J. Phys. Chem. B* **2010**, *114*, 4802–4810.

[24] a) C. Y. Chi, C. Im, V. Enkelmann, A. Ziegler, G. Lieser, G. Wegner, *Chem. Eur. J.* **2005**, *11*, 6833–6845; b) X. H. Zhou, Y. Zhang, Y. Q. Xie, Y. Cao, J. Pei, *Macromolecules* **2006**, *39*, 3830–3840.

[25] S. Destri, M. Pasini, C. Botta, W. Porzio, F. Bertini, L. Marchio, *J. Mater. Chem.* **2002**, *12*, 924–933.

[26] a) F. Cardullo, P. Seiler, L. Isaacs, J. F. Nierengarten, R. F. Haldimann, F. Diederich, T. M. Denti, W. Thiel, C. Boudon, J. P. Gisselbrecht, M. Gross, *Helv. Chim. Acta* **1997**, *80*, 343–371; b) T. Ohno, K. Moriwaki, T. Miyata, *J. Org. Chem.* **2001**, *66*, 3397–3401.

[27] a) D. M. Guldi, C. Luo, A. Swartz, R. Gomez, J. L. Segura, N. Martin, *J. Org. Chem.* **2002**, *67*, 1141–1152; b) A. Gegout, J. F. Nierengarten, B. D. Nicot, C. Duhayon, A. Saquet, A. Listorti, A. Belbakra, C. Chiorboli, N. Armaroli, *Chem. Eur. J.* **2009**, *15*, 8825–8833; c) D. M. Guldi, C. Luo, A. Swartz, R. Gomez, J. L. Segura, N. Martin, *J. Phys. Chem. A* **2004**, *108*, 455–467.

[28] J. P. Lu, J. F. Ding, S. Alem, S. Wakim, S. C. Tse, Y. Tao, J. Stupak, J. J. Li, *J. Mater. Chem.* **2011**, *21*, 4953–4960.

[29] a) B. Knight, N. Martin, T. Ohno, E. Orti, C. Rovira, J. Veciana, J. V. Gancedo, P. Viruela, R. Viruela, F. Wudl, *J. Am. Chem. Soc.* **1997**, *119*, 9871-9882; b) R. Kessinger, J. Crassous, A. Herrmann, M. Rüttimann, L. Echegoyen, F. Diederich, *Angew. Chem.* **1998**, *110*, 2022–2025; *Angew. Chem. Int. Ed.* **1998**, *37*, 1919–1922.

[30] a) J. F. Eckert, J. F. Nicoud, J. F. Nierengarten, S. G. Liu, L. Echegoyen, F. Barigelletti, N. Armaroli, L. Ouali, V. Krasnikov, G. Hadziioannou, *J. Am. Chem. Soc.* **2000**, *122*, 7467–7479; b) A. Molina-Ontoria, G. Fernandez, M. Wielopolski, C. Atienza, L. Sanchez, A. Gouloumis, T. Clark, N. Martin, D. M. Guldi, *J. Am. Chem. Soc.* **2009**, *131*, 12218–12229.

[31] M. W. J. Beulen, L. Echegoyen, J. A. Rivera, M. A. Herranz, A. M. Domenech, N. Martín, *Chem. Commun.* **2000**, 917–918.

[32] U. Hahn, E. Maisonhaute, C. Amatore, J. F. Nierengarten, *Angew. Chem.* **2007**, *119*, 969–972; *Angew. Chem. Int. Ed.* **2007**, *46*, 951–954.

[33] Y. Zhang, Z. Xu, L. Z. Cai, G. Lai, H. Qiu, Y. J. Shen, *J. Photochem. Photobiol. A* **2008**, *200*, 334–345.

[34] a) J. Míšek, A. V. Jentzsch, S. Sakurai, D. Emery, J. Mareda, S. Matile, *Angew. Chem.* **2010**, *122*, 7846–7849; *Angew. Chem. Int. Ed.* **2010**, *49*, 7680–7683; b) C. Ma, M. Fonrodona, M. C. Schikora, M. M. Wienk, R. A. J. Janssen, P. Bäuerle, *Adv. Funct. Mater.* **2008**, *18*, 3323–3331.

[35] a) D. Mi, J. H. Kim, F. Xu, S. H. Lee, S. C. Yoon, W. S. Shin, S. J. Moon, C. J. Lee, D. H. Hwang, *Sol. Energy Mater. Sol. Cells* **2011**, *95*, 1182–1187; b) D. Mi, H. U. Kim, J. H. Kim, F. Xu, S. H. Jin, D. H. Hwang, *Synth. Met.* **2012**, *162*, 483–489.

Received: January 12, 2013
Published online: March 11, 2013